Kristín Martha Hákonardóttir
Tómas Jóhannesson
Felix Tiefenbacher, SLF
Martin Kern, SLF

A laboratory study of the retarding effect of breaking mounds in 3, 6 and 9 m long chutes

A laboratory study of the retarding effect
of breaking mounds in 3, 6 and 9 m long chutes

Kristín Martha Hákonardóttir*, Tómas Jóhannesson,*
Felix Tiefenbacher† and Martin Kern†

May 3, 2001

Abstract

A series of laboratory experiments in 9 m and 3 m long experimental chutes using 100 μm glass particles and 2 mm sand particles, was performed to investigate the effect of scaling of supercritical, high Froude number granular flow interacting with obstacles. The experiments were followup work on laboratory experiments performed in a 6 m long chute in the summer 2000 (Hákonardóttir, 2000), where basic understanding of the retarding effect of avalanche breaking mounds was established. It was verified that the collision of the flow with a row of breaking mounds leads to the formation of a jump or a jet whereby a large fraction of the flow is launched from the experimental chute and subsequently lands back on the chute. The retarding effect of the mounds was investigated quantitatively by direct measurements of the velocity and runout length of the flow along with the geometry of the jet. The effect of several aspects in the layout of the mounds on their retarding effects was examined. It was observed that a row of steep mounds with a height several times the flow depth, a breadth similar to the height and narrow gaps between individual mounds can lead to a $30 - 40\%$ reduction of the runout length of the flow past the mounds.

---

*Icelandic Meteorological Office, Bústaðavegur 9, IS-150 Reykjavík, Iceland.
†Swiss Federal Institute for Snow and Avalanche Research (SLF), Fluelastrasse 11, CH-7260 Davos Dorf, Switzerland.

Contents

1   Introduction

We report on a series of laboratory experiments conducted in order to look at the effect of scaling on rapid granular flows interacting with obstacles. The experiments were carried out in Davos, Switzerland, at the Swiss Federal Institute for Snow and Avalanche Research and in Reykjavík, Iceland, at the Icelandic Meteorological Office. The experiments were performed in collaboration between Switzerland and Iceland as a part of the research project Cadzie which is supported by the European Commision. The aim of the research described here is to establish a fundamental understanding of the retarding effect of avalanche breaking mounds.

The experiments were followup work on small-scale laboratory experiments performed in the summer 2000 at the University of Bristol in England (Hákonardóttir, 2000) and preliminary small-scale experiments conducted earlier at the University (Woods and Hogg, 1999 and Woods and Hogg, 1998). The experiments in Bristol provided a basic understanding of the interaction of high Froude number granular flow with obstacles and the energy dissipation involved in the impact of the flow with the obstacles. They showed that one row of obstacles with a height several times the flow depth, but a height-scale corresponding to only a fraction of the kinetic energy of the flow ($H \ll u^2/(2g)$, where H is the mound height, u is the flow speed and g is the gravitational acceleration), can shorten the runout of the flow by $30-40\%$. These experiments were scaled up by approximately a factor of two in the experiments in Davos, keeping the Froude number of the flow constant. The same small glass particles were used in the current experiments as were used in Bristol. A few experiments were conducted using coarser sand particles in order to investigate the effect of using material of different frictional properties and grain size on the retarding effect of the mounds. In Reykjavík, the Bristol experiments were scaled down by approximately a factor of two again using the same glass particles.

The report is devided into two main sections (§2 and §3). In section 2, the larger scale experiments conducted in Davos are discussed. The experimental setup is described (§2.1) and the results for the ballotini and sand experiments discussed in §2.2. Different techniques to measure the speed of the flow are represented in §2.3, leading to the comparison between basal and surface velocities in the granular current. In section 3, the smaller scale experiments conducted in Reykjavík are described. The experimental results are then compared to the intermediate scale experiments conducted in Bristol earlier (§4) and finally concluding with section 5.

2   Larger scale experiments - Davos

This section describes a series of laboratory experiments performed in a 9 m long chute, where the previous experiments, performed in Bristol, were scaled up by a factor of two.

Material	ρ [kgm^{-3}]	d [mm]	ϕ [°]	δ [°]
Ballotini	1600	0.1	$21 - 23$	$17 - 18$
Sand	1750	2	$31.5 - 33.5$	$25.0 - 27.5$

Table 1: Material properties, ρ is the bulk density of the granular material, d the mean diameter of the particles, ϕ the angle of repose and δ the dynamic bed friction angle.

2.1 Experimental setup

The experiments in Davos were designed so that the particle current had an internal Froude number similar as in the experiments in Bristol which is on the same order of magnitude as for large, dry, natural snow avalanches. The internal Froude number is defined in terms of the flow velocity, u, the depth of the flow, h, and the gravitational acceleration, g, as

$$Fr = \frac{u}{\sqrt{gh}}.$$

It represents the square root of the ratio of the kinetic energy of the current to the potential energy of the flow, or the ratio of the flow velocity to the speed of free surface gravity waves in the flow. The Froude number in the experiments was $Fr \sim 10$. The flow front could easily be tracked down the chute and the speed in the interior of the flow was measured by tracing irregularities in the flow by means of optical velocity censors and a high speed camera, see §2.3. The frame grabber of the video machine used in analysing the experiments accessed 25 frames per second, while the high speed camera accessed 5000 frames per second.

Model barriers were designed so that the ratio of the height of the barriers to the flow depth was between 1 and 5. The barrier Froude number is defined in terms of the flow velocity and the height of the barriers, H, as

$$Fr_b = \frac{u}{\sqrt{gH}},$$

and represents the square root of the ratio of the kinetic energy of the current to half the potential energy corresponding to the height of the barriers. The Froude number of the barriers in the experiments was in the range $5 < Fr_b < 10$.

The laboratory experiments were performed on a 9 m long wooden chute consisting of two straight sections (Fig. 1). The slope of the upper section was 45° and that of the lower section about 10°. A row of obstacles was located on the lower section, 15 cm downstream from the top of the lower section. The barriers were constructed of wood and had heights, H, of 2.5, 3, 5 and 10 cm and widths, B, of 5, 10 and 15 cm, with the upstream face perpendicular to the chute (Fig. 2).

Almost spherical, glass ballotini particles were used in the experiments as well as sand particles.
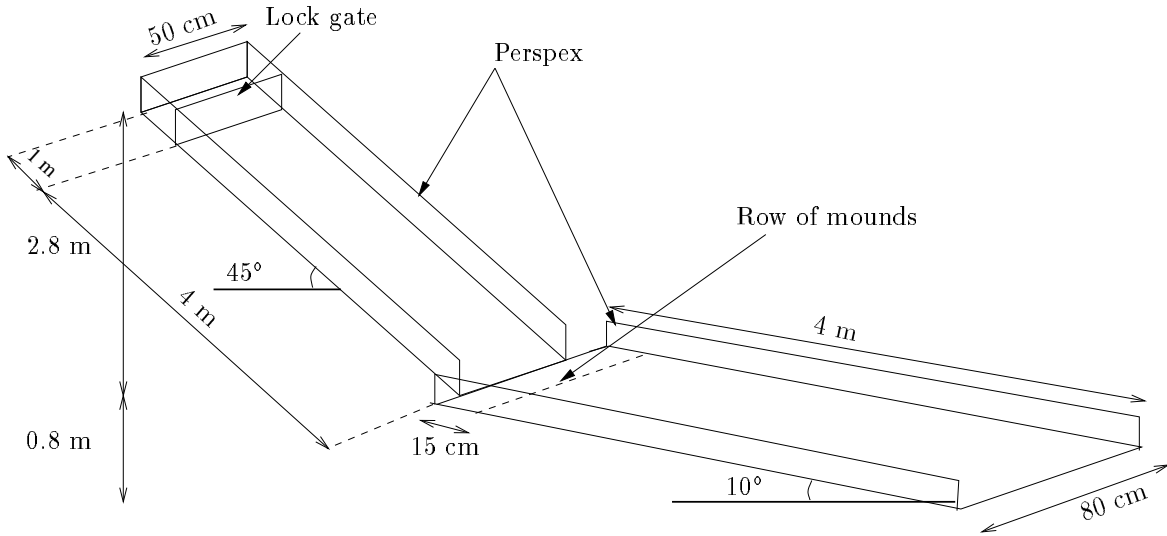
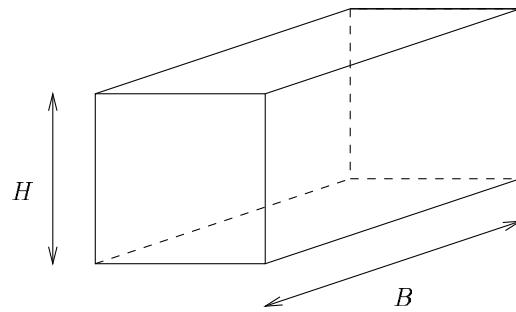Figure 1:   Schematic diagram of the chute.

Figure 2:   Schematic diagram of a mound.

In each experiment, a measured amount of particles was released from the top of the chute. The motion down the slope was recorded by video and subsequently analysed, and the runout length and distribution of the deposited particles, averaged over the width of the chute, was measured. In order to simplify the organisation of the experiments, a datum configuration of the mound geometry, avalanche size, *etc.* was defined. It consisted of a mass of 50 kg and 3 elongated mounds covering 60% of the cross sectional area of the upper section of the chute. The mounds had a height of 5 cm (approximately twice the flow depth) and were 10 cm wide, see Figure 3. Experiments with mounds were compared to a control run, where no obstacles were used.
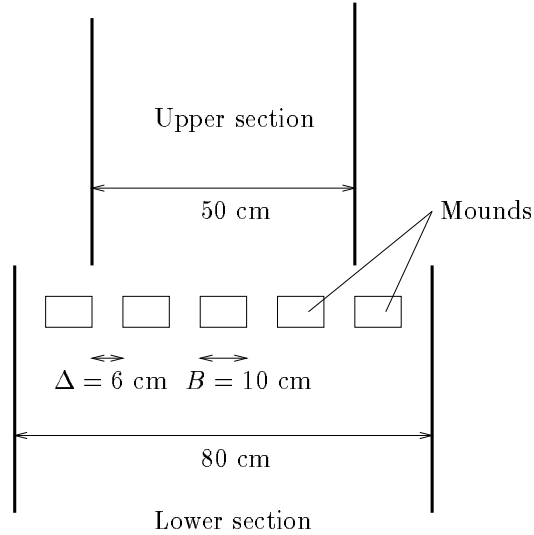
The experiments conducted are summarised in Table 2.

Figure 3:   Schematic diagram of the datum mound configuration, plan view.

Experiment	Ballotini	Sand	H [cm]	B [cm]	Δ [cm]	A	H/B
Low dam	x		2.5	-	-	1.0	-
Low dam		x	3.0	-	-	1.0	-
Dam	x	x	5	-	-	1.0	-
High dam	x		10	-	-	1.0	-
Datum mounds	x	x	5	10	6	0.6	0.5
Narrow mounds	x	x	5	5	3	0.6	1.0
Low mounds	x		2.5	5	3	0.6	0.5
High, wide mounds	x		10	15	10	0.6	0.67
Smaller rel. area	x		5	10	15	0.4	0.5
Two rows	x	x	5	10	6	0.6	0.5
Conical mounds	x	x	5	10	0	0.5	0.5

Table 2: The experiments conducted. A is the proportion of the cross sectional area of the upper section of the chute covered by mounds.

2.2   Results

It was observed that a row of barriers leads to a significant decrease in the runout length of the flow downstream of the obstacles, relative to a flow without barriers. The granular current, passing over the obstacles forms an airborne jet that is launched from the top of the obstacle. The jet travels a considerable distance downslope before landing back on the chute. Thereafter it resumes downslope motion along the chute.

2.2.1 Control experiment

Ballotini

The control experiment with no barriers consisted of releasing 50 kg of material down the chute and resulted in a runout, $x_{cont} = 3.90$ m, measured from the point where the row of obstacles was placed in the experiments with obstacles.
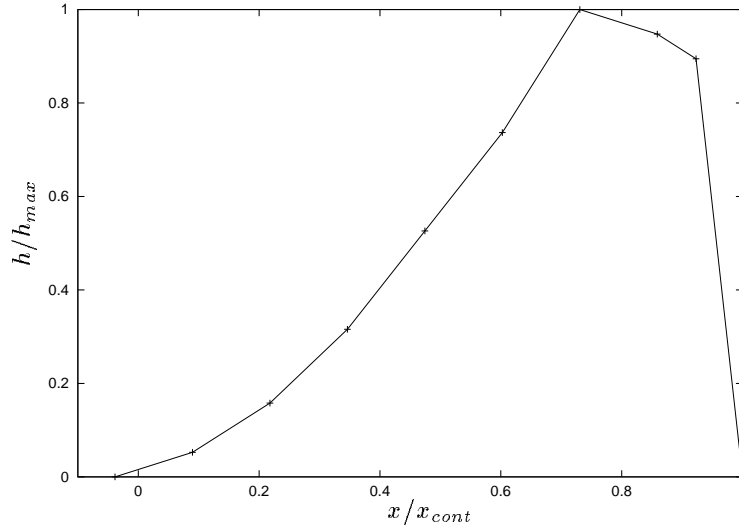

Figure 4: Averaged non-dimensional length profile of the deposit of ballotini on the lower section for the control run, measured from the start of the lower section and plotted relative to the maximum runout, x_{cont}.

The particle current, traveling down the upper section of the chute, quickly reached a terminal speed close to 5 ms^{-1}, which remained constant until the slope angle changed. The current traveled with the shape of a parabolic cap, with a quasi-steady maximum flow depth of 2.25 cm, corresponding to an internal Froude number of approximately 11. The flow started decelerating on the lower section and came to rest near the end of the section (Fig. 4).

Sand

The control experiment for the sand also consisted of releasing 50 kg of material down the chute and resulted in a runout, $x_{cont} = 3.25$ m measured from the point where the row of obstacles was placed in the experiments with obstacles.

The particle current, traveling down the upper section of the chute, reached a terminal speed close to 5.3 ms^{-1}, which remained constant until the slope angle changed. The current traveled with the shape of a parabolic cap, with a quasi-steady maximum flow depth of 3.0 cm, corresponding to an internal Froude number of approximately 10. The averaged non-dimensional length profile of the deposit of sand on the lower section of the chute is displayed
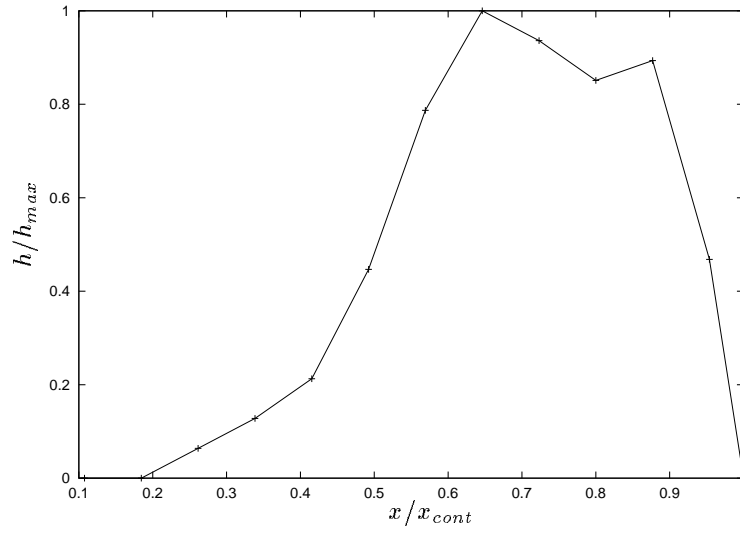
11

Figure 5: Averaged non-dimensional length profile of the deposit of sand on the lower section for the control run, measured from the start of the lower section and plotted relative to the maximum runout, x_{cont}.

in Figure 5.

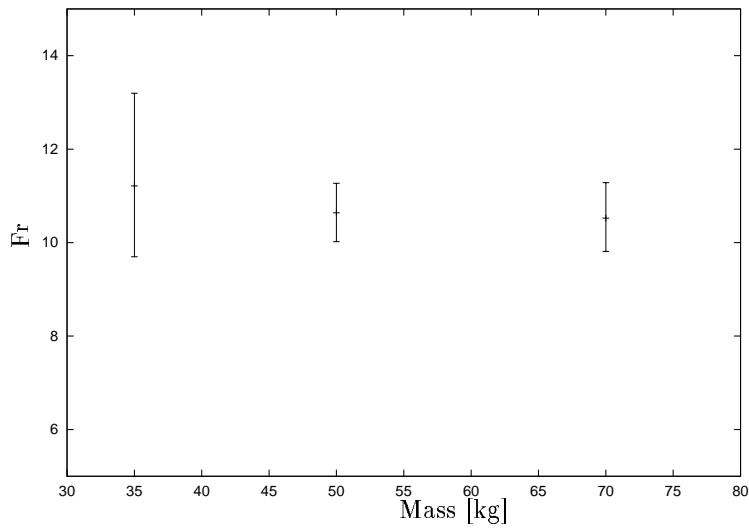## 2.2.2 Flow without mounds

Figure 6: Change in the internal Froude number of the ballotini particle current for different mass of material released, measure on the upper chute after the stream had reached a semi-steady state.

The effect of varying the total mass of material released, on the internal Froude number of the flow of ballotini particles on the upper section, was investigated for flow without barriers. The Froude number, once the flow had reached a quasi-steady state on the upper section of the chute, was found to be relatively independent of the amount of material released, see Figure 6. The speed of the flow front varied from about 4.5 ms^{-1} for 35 kg of ballotini to about 5.5 ms^{-1} for 70 kg and the maximum flow depth from about 1.9 cm for 35 kg to about 2.5 cm for 70 kg. The Froude number was found to be in a relatively narrow range for comparatively large variations in the amount of material released and in the respective speed of the flow. This, along with the fact that the flow reached an approximate steady state on the upper section, suggests that a turbulent drag force depending on the square of the velocity affects the motion of the current in addition to a Coulomb drag force proportional to the weight of the material and the downslope gravitational acceleration (see Hákonardóttir, 2000 for further discussion).

2.2.3 Flow with mounds

Ballotini

Experiment	runout, x [m]	x/x_{cont}	cm runout, $x^{cm}[m]$	x^{cm}/x^{cm}_{cont}
Low dam	3.58	0.92	1.95	0.73
Dam	2.60	0.67	1.15	0.43
High dam	2.10	0.54	0.75	0.28
Datum mounds	3.01	0.77	1.64	0.61
Narrow mounds	2.60	0.67	1.43	0.53
Low mounds	3.35	0.86	2.05	0.76
High mounds	2.70	0.69	1.15	0.43
Smaller rel. area	3.14	0.81	1.92	0.72
Two rows	2.45	0.63	1.32	0.49
Conical mounds	3.29	0.84	2.11	0.79

Table 3: Summary of the experiments conducted. The runout was measured from where the row of obstacles was placed, x_{cont} is the runout of the control run, x^{cm} is the center of mass runout and $x^{cm}_{cont} = 2.68$ m, also measured from where the row of obstacles was placed.

It can be assumed that the flow had slowed down somewhat and thickened before hitting the row of mounds on the lower section of the chute, leading to a slightly lower Froude number than on the upper section, *i.e.* $Fr \approx 8 - 9$.

The non-dimensional runout, x/x_{cont} is plotted against the non-dimensional height of the dams in Figure 7 for the experiments summarised in Table 3. For the dams, the runout decreased with increasing height of the dam. Increasing the height of the mounds to more
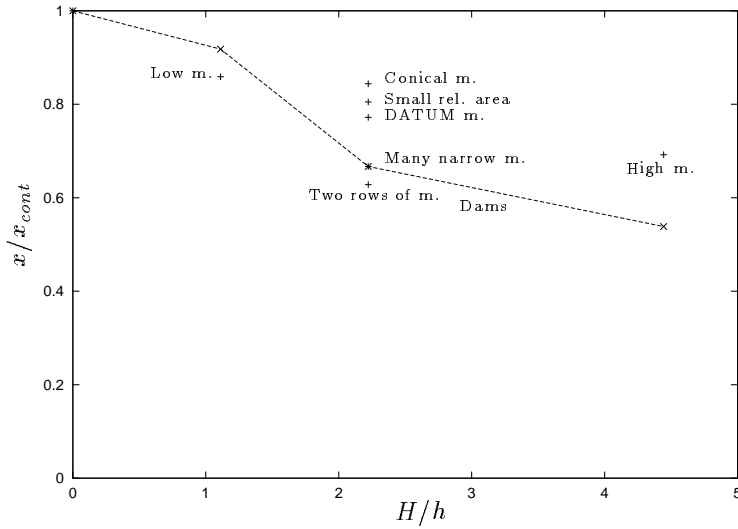
Figure 7: Non-dimensional runout, x/x_{cont} for the ballotini plotted against non-dimensional height of the obstacles, H/h.

than twice the flow depth did, on the other hand, not lead to further reduction in the runout (see Hákonardóttir, 2000 for explanation). For the low retarding structures (height similar to the thickness of the flow), the mounds were more effective than a continuous dam of the same height. Also, narrow mounds with many gaps inbetween were more effective than wide mounds with fewer gaps, covering the same cross sectional area. Figure 7 also shows that one row of the most effective configuration of 5 cm high mounds shortens the runout by about 30%, which is the same reduction of runout as for a continuous dam of the same height. It is interesting to note that the most common shape of mounds, *i.e.* traditional conical mounds, is the least effective configuration and that two rows of mounds are not as effective as one might conclude from the effectiveness of a single row.

The depth-averaged length profiles were plotted for all the runs (see appendix A.1). From the profiles, we see that the bulk of the material is deposited higher upstream on the chute for the mound experiments than the deposit of the control run. It is therefore of interest to look at the location of the centre of mass of the deposits with obstacles relative to the centre of mass for the control run. Figure 8 illustrates that the higher the obstacles, the further upstream the centre of mass is deposited. A continuous dam is more effective in shortening the centre of mass runout than a row of mounds for all heights and geometries of obstacles. Also, the centre of mass runout is in all cases shortened more than the maximum runout of the flow. The conical mounds are still the most ineffective configuration and two rows of mounds are the most effective configuration for a mound height of 5 cm, since most of the deposit is left upstream of the lower row of mounds and the material near the front is very thin.
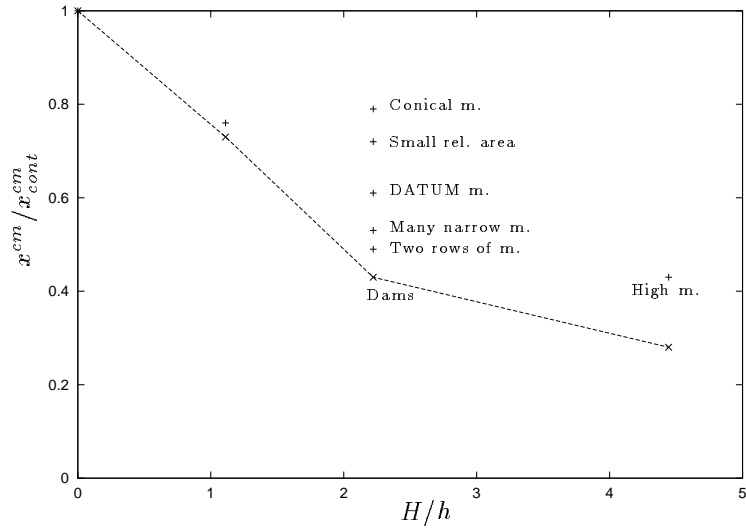
Figure 8: Non-dimensional centre of mass runout, x^{cm}/x^{cm}_{cont} for the ballotini plotted against non-dimensional height of the obstacles, H/h.

In the experiments in Bristol, the jet of particles jumping over the mounds and dams, could be treated like a projectile motion in two dimensions (Fig. 9):

$$\mathbf{F} = m\mathbf{g} - mk\dot{\mathbf{x}}|\dot{\mathbf{x}}|,$$

where $\mathbf{F}$ is a force exerted on the mass m, $\mathbf{g}$ is the gravitational acceleration and k is a dimensional constant representing the drag, subject to the initial conditions

$$z = x = 0 \qquad \text{at} \qquad t = 0$$

and

$$\dot{x}(0) = u_1 \cos \theta_1,$$
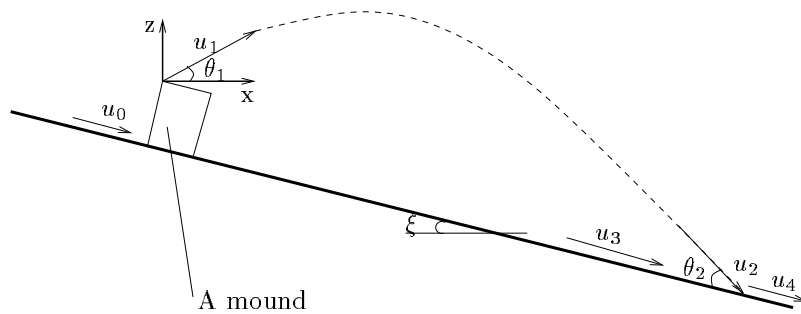
Figure 9: Sideview of a jet.

15

$$\dot{z}(0) = u_1 \sin\theta_1.$$

In Bristol, it was found that the geometry of the jet was best explained by neglecting the air resistance represented by the coefficient k. By taking $k = 0$, the solution to the system above is

$$x = u_1 \cos\theta_1 t, \qquad (1)$$

$$z = u_1 \sin\theta_1 t - \frac{1}{2}gt^2, \qquad (2)$$

and the equation for the trajectory of the jet is

$$z = x\tan\theta_1 - \frac{1}{2}\frac{gx^2}{u_1^2}\sec\theta_1.$$

This also happened to be the case for the ballotini experiments in Davos, described in this report.

The oncoming speed, u_0, was estimated from the steady speed on the upper section of the chute, to be $u_0 = 4$ ms^{-1}. The trajectory of the jet was measured in each experiment. The parameters that define the geometry of the quasi-steady jet are the throw angle, θ_1, and the velocity, u_1. It was hard to measure θ_1 and u_1 directly from the video recordings since a cloud of particles obstructed a clear vision of the throw. They could nevertheless be calculated indirectly as follows. The trajectory of the jump was very well defined in the experiments, thus a parabola $z = ax - b^2 x^2$ could be fitted to the trajectory using the method of least squares. Hence,

$$\theta_1 = \arctan a,$$

$$u_1 = \frac{\sec\theta_1}{b}\sqrt{\frac{g}{2}}.$$

Since u_1 and θ_1 are interdependent, an error in a leads to an error in the throw angle, θ_1, which adds to the already existing error in u_1 caused by inaccuracy in b.

The jets for the runs with dams were drawn from the video recordings and moved into the coordinate system illustrated in Figure 9. Parabolas were then fitted to the points, see Figure 10. These jets have important practical consequences for the use of multiple rows of mounds to retard avalanches. The spacing between the rows must be chosen sufficiently long so that the material launched from the mounds does not jump over rows further down the slope in order for the lower rows to have full retarding effect.

An understanding of the factors that control θ_1 and u_1 is fundamental to be able to predict the trajectory of the jet. The throw angle, $\theta_1 + \xi$ (ξ is the angle between the chute and horizontal, defined in Figure 9), calculated as described above, is plotted against the non-dimensional height of the mounds, H/h, in Figure 11. As the height of the mounds increases, θ_1 becomes larger and the particle current jumps under a steeper angle.
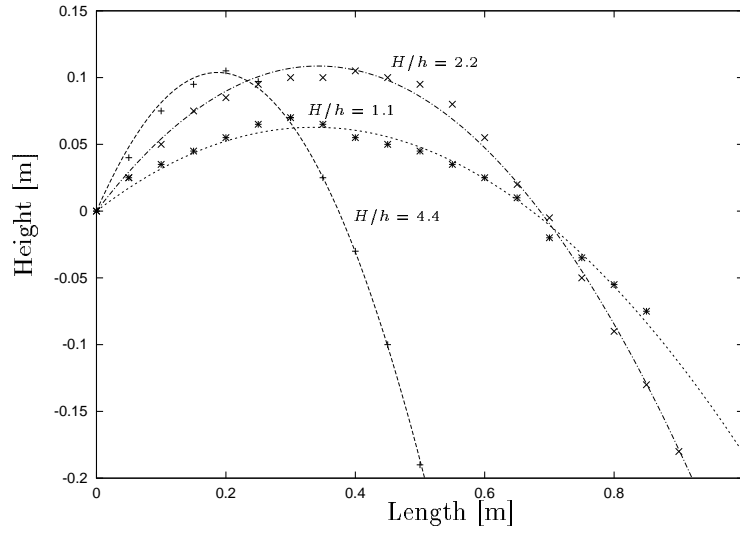
16

Figure 10: Jet profiles for 2.5, 5.0 and 10.0 cm high dams.
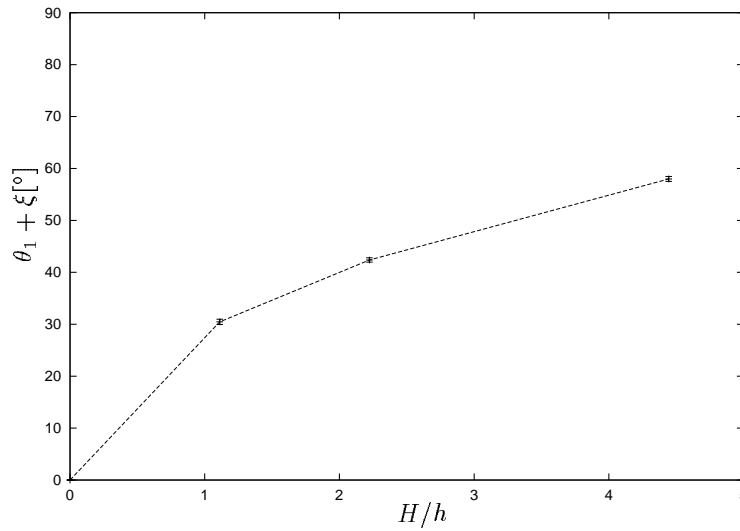

Figure 11: The throw angle, $\theta_1 + \xi$ plotted against the non-dimensional height of the obstacles, H/h, for the dams.

A considerable amount of energy is dissipated when the flow hits the mounds and lands again on the chute. The ratio u_1/u_0 represents the speed reduction in the initial impact with the obstacles. If no energy is lost in the collision, simple energy conservation gives
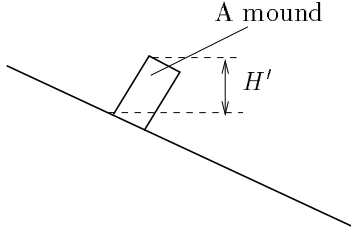
$$\frac{1}{2}u_1^2 = \frac{1}{2}u_0^2 - gH',$$

17

Figure 12: The height, H' defined, sideview of a mound.

where H' is defined in Figure 12. Hence,

$$\frac{u_1}{\sqrt{u_0^2 - 2gH'}} = 1. \tag{3}$$

Plotting this ratio provides an estimate of the amount of energy dissipated in the impact and the process of turning the flow (Fig. 13). The use of H' leads to the largest possible decrease in the kinetic energy due to an increase in potential energy. This is not entirely correct since it was observed that a wedge is formed upstream of the mounds reducing the effective height of the mounds, H'. This may lead to a small underestimate of the energy dissipation. Figure 13 illustrates that a substantial fraction of the energy was dissipated in the impact. The velocity was lowered by around 20% for a non-dimensional dam height of 1. Further increase in the dam height leads to further lowering of the velocity and the velocity was reduced by about
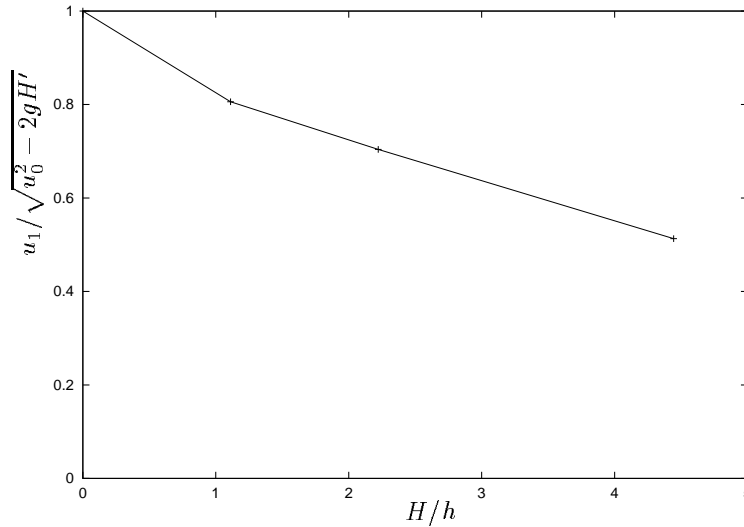
Figure 13: The ratio in equation (3) plotted against the non-dimensional height H/h for the dams.

50% for a non-dimensional dam height of 4.4. The energy dissipation can be explained by the

fact that grain-grain collisions in the flow, which may be expected to become more frequent due to an interaction of the flow with the mounds or a dam, do not conserve kinetic energy. The coefficient of restitution, ϵ, was measured to be $\epsilon = 0.8$ for 350 μm glass ballotini. This value may be expected to give a reasonable estimate of the coefficient for the 100 μm ballotini.

It was observed in the experiments in Bristol that a row of mounds lowered the velocity u_1 in a broadly similar way as a dam for mound heights $H/h \leq 2$, and the throw angle, $\theta_1 + \xi$ was similar to that of a dam for all mound heights. The jet trajectories were similar to those for dams for the lower mounds, but the formation of a wedge upstream of the mounds introduced a three dimensionality in the jets leading to a slight shortening of the length of the trajectory along the chute.

Sand

Experiment	runout, x [m]	x/x_{cont}	cm runout, $x^{cm}[m]$	x^{cm}/x^{cm}_{cont}
Low dam	2.00	0.61	1.16	0.55
Dam	1.65	0.51	0.59	0.27
Datum mounds	2.55	0.78	1.38	0.66
Narrow mounds	1.95	0.60	1.10	0.53
Two rows	1.70	0.52	0.52	0.25
Conical mounds	2.05	0.63	1.33	0.63

Table 4: The experiments conducted using sand. The runout was measured from where the row of obstacles was placed, x_{cont} is the runout of the control run, x^{cm} is the center of mass runout and $x^{cm}_{cont} = 2.09$, also measured from where the row of obstacles was placed.

It can be assumed for the sand like for the ballotini that the flow had slowed down somewhat and thickened before hitting the row of mounds on the lower section of the chute, leading to a slightly lower Froude number than on the upper section, *i.e.* $Fr \approx 7 - 8$.

The non-dimensional runout, x/x_{cont} is plotted against the non-dimensional height of the obstacles in Figure 14 for the experiments summarised in Table 4. We see that the runout for the dams shortens with increasing height as for ballotini. A non-dimensional dam height of 1.7 shortens the runoutlength by about 50%. For the mounds, two rows are most effective and shorten the runout by the same amount as a dam for $H/h = 1.7$. It is interesting to note that both many narrow mounds and conical mounds are more effective than the datum mound configuration.

The depth-averaged length profiles were plotted for all the runs (see appendix A.2). From the profiles we see that the bulk of the material is deposited higher upstream on the chute for the mound experiments than the deposit of the control run. We therefore look at the location of the centre of mass of the deposits with obstacles relative to the centre of mass for the control run. Figure 15 illustrates that the higher the obstacles the further upstream the
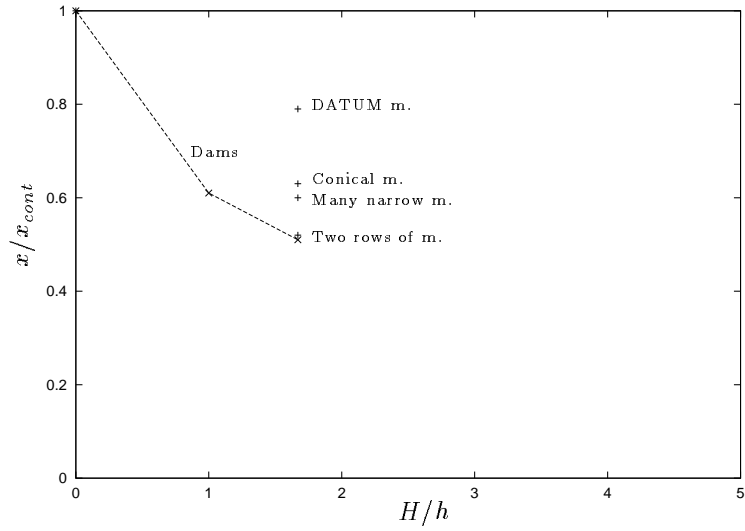
19

Figure 14: Non-dimensional runout, x/x_{cont} for sand plotted against non-dimensional height of the obstacles, H/h.
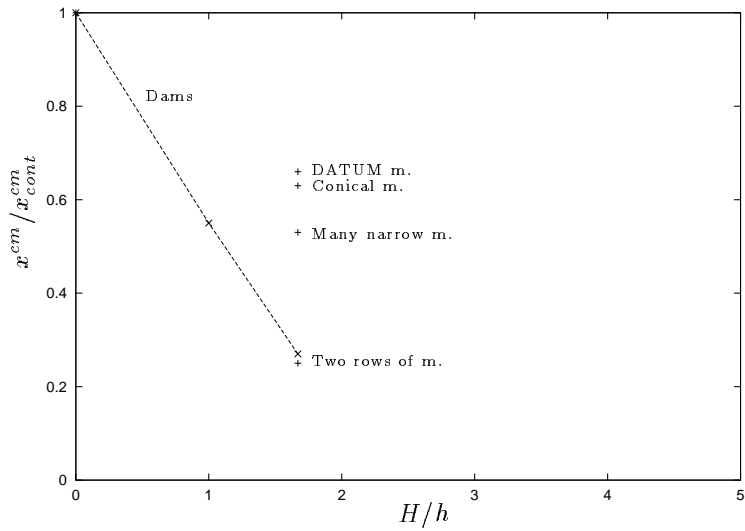

Figure 15: Non-dimensional centre of mass runout, x^{cm}/x^{cm}_{cont} for sand plotted against non-dimensional height of the obstacles, H/h.

centre of mass is deposited. Two rows of mounds are still the most effective configuration and have similar effect as a dam of the same height. The effect of the conical mounds is similar to the datum mound configuration. The centre of mass runout is in all cases shortened more than the maximum runout of the flow.

2.3 Speed measurements

Two methods were used to measure the speed of the current. Optical sensors in the sliding surface of the chute were used to measure the basal velocity of the flow, v_0, and a high speed camera with a record rate up to 5000 frames per second was used to determine the speed of the material at the surface of the flow, v_s.

2.3.1 Optical velocity sensors

The speed of the flow was obtained by using a measurement procedure based on optical reflection. A new generation of optical sensors was developed, based on the design originally proposed at Montana State University (Dent et al., 1997). The optical sensor consists of two photo diode/photo transistor pairs. The photo diode emits infrared light and the photo transistor detects the reflected infrared light. If a reflecting object moves over the sensor, the photo transistor supplies a voltage signal as a function of the intensity of the reflected light. Using a bandpass filter, only the intensity variations are recorded by the data acquisition system (a PC with a National Instruments PCI DAQ card).
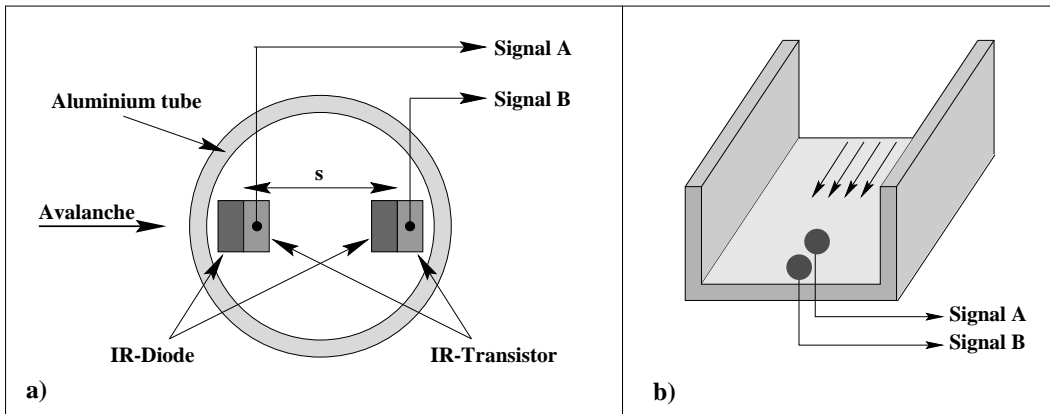
Figure 16: a) Top view of an optical speed sensor. The tube also contains the electronics running the sensors. b) The optical sensors are mounted flush to the sliding surface of the chute. s is the spacing between the the diode/transistor pairs.

The sensors were placed in aluminium tubes covered with transparent perspex disks with a fixed distance between the diode/transistor pairs. The tubes were inserted flush to the sliding surface of the chute, see Figures 16 and Figure 18a).

When granular material flows over an optical sensor, each transistor pair submits a voltage signal as a function of the instantaneous internal structure of the granular material. Due to the fact that the internal structure of the flow is constant over a certain distance, the output signals of each pair are similar but time shifted by
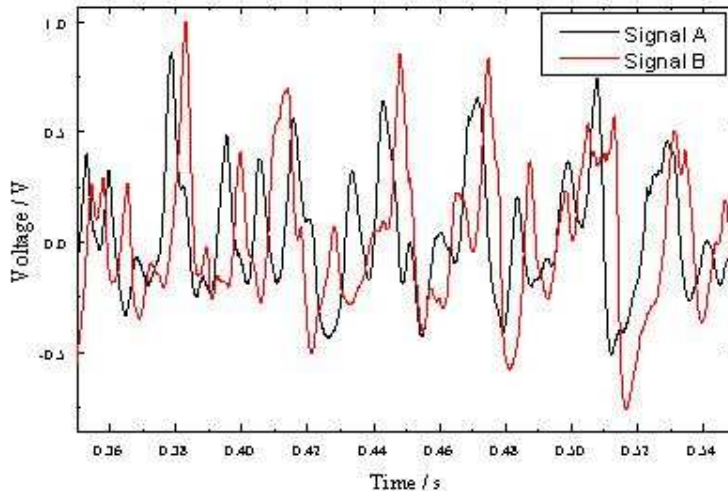
$$\Delta t = s/v,$$

21

Figure 17: Signal A (upper pair) and B (lower pair) from the optical sensors. Signal B has a similar form to signal A, but is time shifted.

where v is the flow velocity and s the spatial distance between the two pairs (see Figure 17).

Both the data acquisition and the analysis software were programmed in LabVIEW (National Instruments). In the analysis, a cross correlation function

$$S(\tau) = \int A(t) \cdot B(t + \tau) dt$$

is formed from the sensor output functions $A(t)$ and $B(t)$. This function shows for which time shift, $\tau_{\max}$, the correlation of the signals is optimal. Hence the flow velocity can be calculated

$$v = \frac{s}{\tau_{\max}}.$$

2.3.2 Measurements with a high speed camera

To investigate the influence of friction between the granular flow and the sliding surface of the chute, the speed at the surface was measured using a high speed camera (see Figure 18). The camera could record up to 5000 frames per second but its memory was limited to 512 frames. The opening time of the shutter, t_s was adjusted in the range of $t_s \epsilon [500 \ s^{-1}; 1250 \ s^{-1}]$. An experiment on the chute takes between one and two seconds, so that a rate of 250 frames per second was used. The films were analysed using WinAnalyse, by tracking surface structures of the flows (for the experiments using ballotiny, marker particles were tracked), and the velocity of the flow calculated as a function of time directly above the optical sensors.

Comparing the velocities (see Figures 19 and 20) we see that friction reduces the speed at the bottom by about 1 ms^{-1} for the ballotini and by about 0.5 ms^{-1} for sand compared to the speed near the surface of the flow.
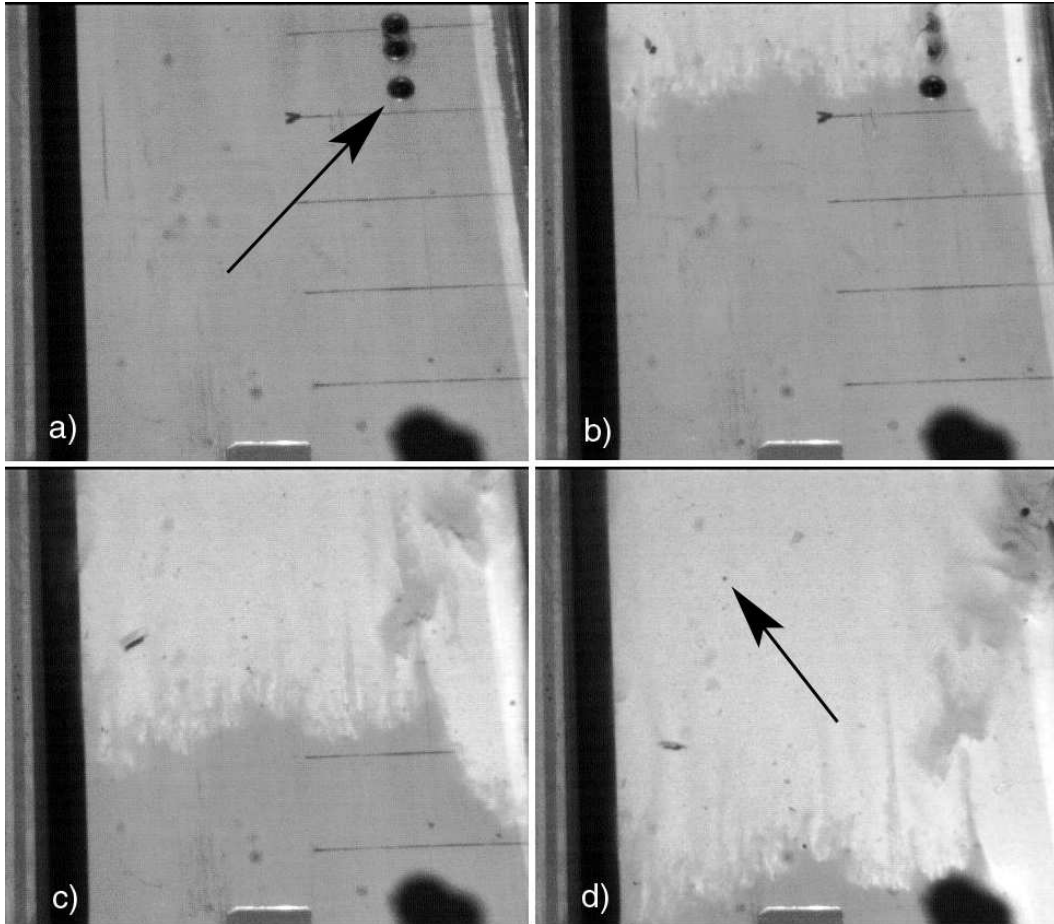
Figure 18: Pictures from the high speed camera. In a) the optical sensors built in the sliding surface of the chute are shown. In d) the arrow points to one of the marker particles we mixed into the ballotini to measure the speed. For the sand experiments we did not need marker particles because the sand avalanches have enough internal optical structure for tracking.

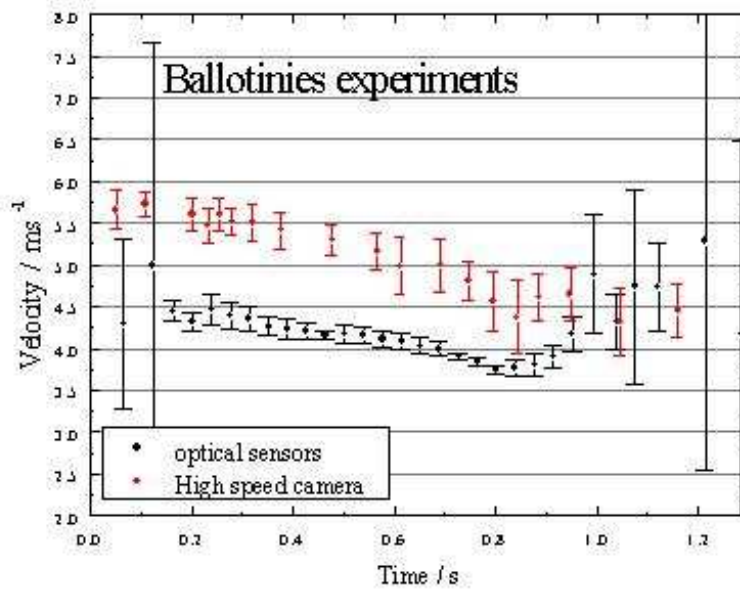### 2.3.3 Comparison between basal and surface velocities

Figure 19: Velocity at the sliding surface of the chute compared to the surface velocity for the ballotini experiments. One can see clearly that the friction at the sliding surface reduces the basal velocity.

Looking at the data from the optical speed sensors, three phases of the flow can be distinguished: 1) the main flow, 2) the final stages of the main flow and 3) the rest. The main flow is characterised by a quite stable behavior of flow depth and velocity, which lasts for about half a second when a decrease of the basal velocity occurs. The velocity decrease is a consequence of the thinning of the flow towards the end. This decrease is clearly visible in figures 19 and 20. The end of the main flow can be seen at 0.8 s for the ballotiny and 0.6 s for the sand. When the bulk of the flow has passed, the remaining material creates a shallow flow over the sensors. The thickness is about 2-5 particle layers (4 mm for the sand) and the particles are jumping down the chute almost frictionless, leading to an increase in the flow velocity. At this stage, no difference can be detected between the basal and surface velocities.

3 Smaller scale experiments - Reykjavík

In this smaller scale experimental series, the experiments in Bristol were scaled down by a factor of two using a 3 m long chute.
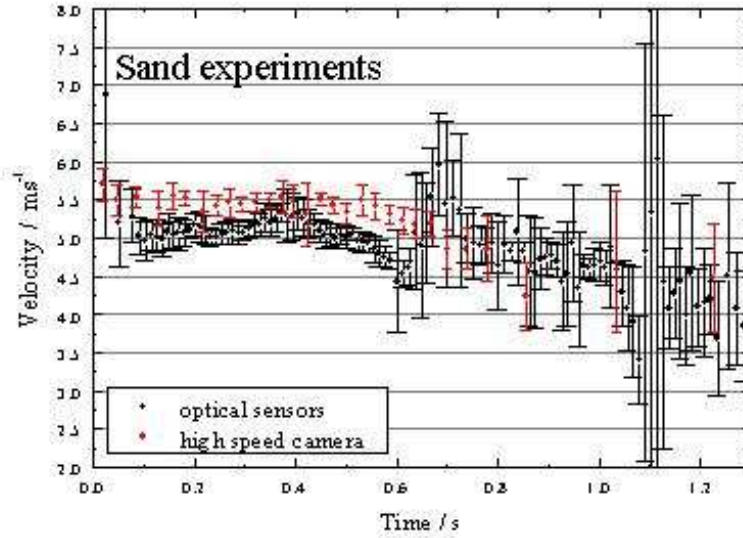
Figure 20: Velocity at the sliding surface of the chute compared to the surface velocity for the sand experiments.

3.1 Experimental setup

The experiments in Reykjavík were designed in the same way as those in Davos. The particle current had an internal Froude number ~ 10. The flow front was tracked down the chute by a video camera. The frame grabber of the video machine used in analysing the experiments accessed 50 frames per second.

Model barriers were designed so that the ratio of the height of the barriers to the flow depth was between 1 and 4. The Froude number of the barriers in the experiments was in the range $6 < Fr_b < 12$.

The laboratory experiments were performed on a 3 m long wooden chute consisting of two straight sections (Fig. 21). The slope of the upper section was 43° and that of the lower section about 14°. A row of obstacles was located on the lower section, 2.5 cm downstream from the top of the lower section. The barriers were constructed of wood and had heights, H, of 0.5, 1, 1.5 and 2 cm and widths, B, of 1, 2 and 3 cm, with the upstream face perpendicular to the chute (Fig. 22). Upstream faces of 60° and 30° were also tried for the narrow mound configuration, described in table 6. Almost spherical, glass ballotini particles were used in the experiments, see table 5 for material properties.

In each experiment, a measured amount of particles was released from the top of the chute. The motion down the slope was recorded by video and subsequently analysed, and the runout length and distribution of the deposited particles, averaged over the width of the chute, was
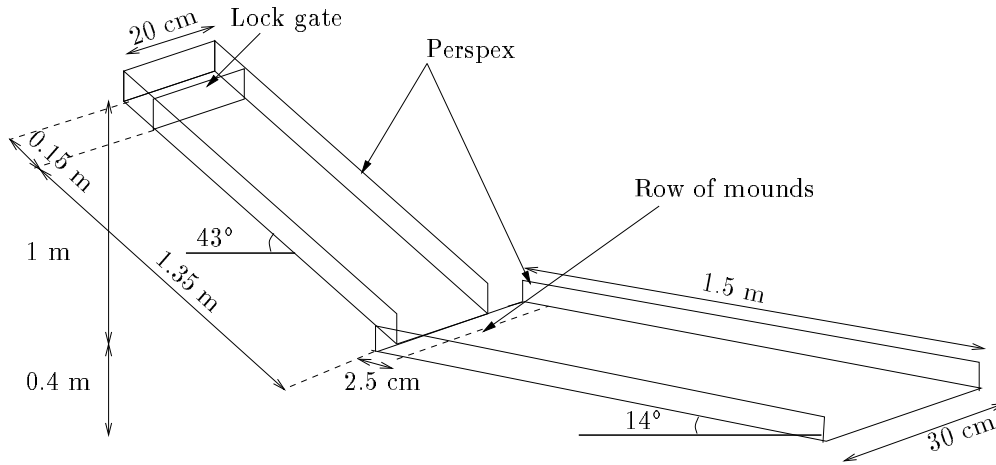
25

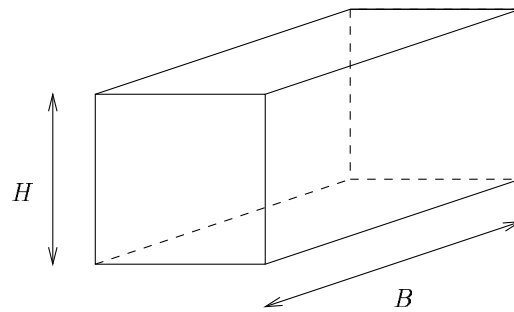Figure 21:   Schematic diagram of the chute.

Figure 22:   Schematic diagram of a mound.

measured. In order to simplify the organisation of the experiments, a datum configuration of the mound geometry, avalanche size, *etc.* was defined. It consisted of a mass of 2 kg and 6 elongated mounds covering 60% of the cross sectional area of the upper section of the chute. The mounds had a height of 1 cm (approximately twice the flow depth) and were 2 cm wide, see Figure 23. Experiments with mounds were compared to a control run, where no obstacles were used.

The experiments conducted are summarised in Table 6. Mounds designed as a part of avalanche protection measures below the gully Drangagil above the town Neskaupstaður in eastern Iceland have a trapizoidal geometry. This type of mounds was therefore also tested in the experiments (Fig. 24).

26

Material	ρ [kgm^{-3}]	d [mm]	ϕ [°]	δ [°]
Ballotini	1600	0.1	$21 - 23$	$19 - 21$

Table 5: Material properties, ρ is the bulk density of the granular material, d the mean diameter of the particles, ϕ the angle of repose and δ the dynamic bed friction angle.
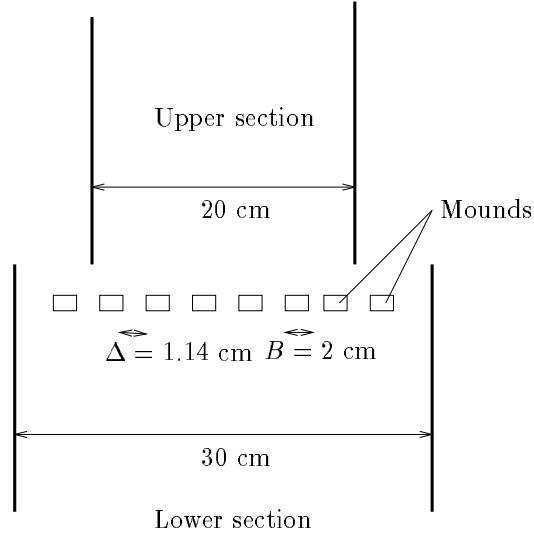
Figure 23: Schematic diagram of the datum mound configuration, plan view.

3.2 Results

3.2.1 Control experiment

The control experiment with no barriers consisted of releasing 2 kg of material down the chute and resulted in a runout, $x_{cont} = 1.22$ m, measured from the point where the row of obstacles was placed in the experiments with obstacles. The particle current reached a semi-steady state on the upper section of the chute just before reaching the lower section. The current travelled in a parabolic shape as observed in the larger scale experiments and came to a rest on the lower section, with the first front reaching furthest and particles flowing on top of material already at rest (Fig. 25).

3.2.2 Flow without mounds

The effect of varying the total mass of material released, on the internal Froude number of the flow of ballotini particles on the upper section, was investigated for flow without barriers. The Froude number was found to vary slightly with the amount of material released and not stay constant as observed in Bristol and Davos. This might be a consequence of the flow not having

Experiment	H [cm]	B [cm]	Δ [cm]	A	H/B
Low dam	0.5	-	-	1.0	-
Dam	1.0	-	-	1.0	-
High dam	1.5	-	-	1.0	-
Higher dam	2.0	-	-	1.0	-
Datum mounds	1.0	2.0	1.14	0.6	0.5
Narrow mounds	1.0	1.0	0.61	0.6	1.0
Low mounds	0.5	1.0	0.61	0.6	0.5
High	1.5	3.0	1.60	0.6	0.5
Smaller rel. area	1.0	2.0	2.4	0.4	0.5
Two rows	1.0	2.0	1.14	0.6	0.5
Conical mounds	1.0	2.0	0	0.5	0.5
Trapizoidal mounds	1.0	3.0	0	0.6	0.5

Table 6: The experiments conducted. A is the proportion of the cross sectional area of the upper section of the chute covered by mounds.

completely reached a semi-steady state before hitting the mounds, or the channalisation and basal friction effecting the flow more than for the larger scales in Bristol and Davos.

3.2.3 Flow with mounds

Two photographs of experiments with mounds in the 3 m chute are shown in Figure 27. The non-dimensional runout, x/x_{cont} is plotted against the non-dimensional height of the mounds in Figure 28 for the experiments summarised in Table 7. Again we see that increasing the height of the mounds shortens the runout of the current until the mounds have reached a height about twice that of the thickness of the current. Increasing their height beyond that does not lead to a significant reduction in the runout. The dams, on the other hand continue to shorten the runout of the current when their height is increased more than this. Like before, low mounds ($H/h < 2$) are more effective than low dams. The conical mounds are still the most ineffective mound geometry and narrow mounds the most effective for the same mound height and area covered. The trapizoidal mounds lead to a very similar reduction in the runout as the datum mounds.

The effect of the obstacles in the flow path becomes greater when looking at the runout of the center of mass (Fig. 29). We still see the same trends, i.e. the conical mounds are least effective and the narrow mounds reduce the runout by the biggest amount for the same height and area covered.

The effect of changing the upstream angle of the mounds, α, on the runout of the stream for a 2 kg release is plotted in Figure 30. The narrow mound configuration was used. We see that steeper upstream angles are more effective than less steep angles.
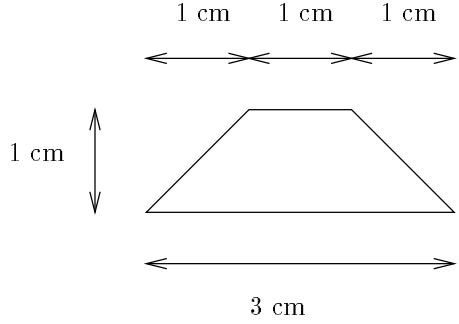
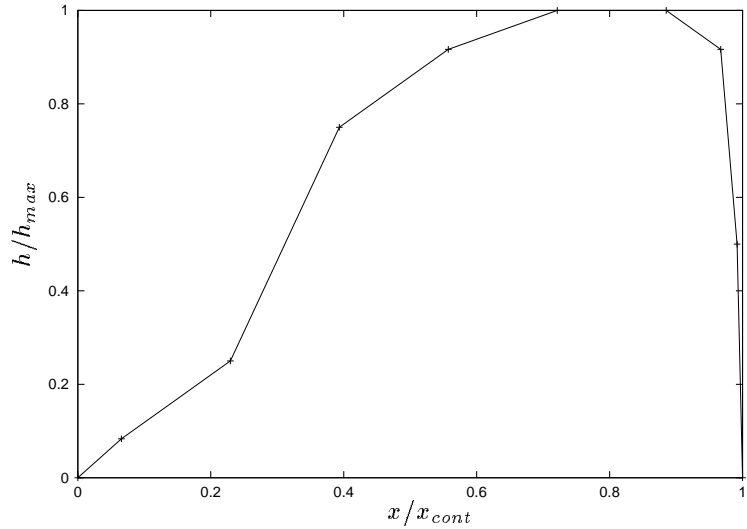Figure 24: A schematic diagram of trapizoidal mounds.

Figure 25: Averaged non-dimensional length profile of the deposit of ballotini on the lower section for the control run, measured from the start of the lower section and plotted relative to the maximum runout, $x_{cont} = 1.22$ m.

The jets of particles over the dams were drawn from the video recordings and moved into the coordinate system illustrated in Figure 9. Parabolas were then fitted to the points, see Figure 31. The throw angle, $\theta_1 + \xi$, calculated as described in section 2.2.3, is plotted against the non-dimensional height of the mounds, H/h, in Figure 32. As the height of the mounds increases, θ_1 becomes larger and the particle current jumps under a steeper angle.

The ratio u_1/u'_0, where $u'_0 = \sqrt{u_0^2 - 2gH'}$, defined in equation (3) represents the energy dissipation in the impact with the mounds and the process of turning the flow. Figure 33 illustrates that a substantial fraction of the energy was dissipated in the impact. The velocity was lowered by around 40% for a non-dimensional dam height close to 1. This reduction
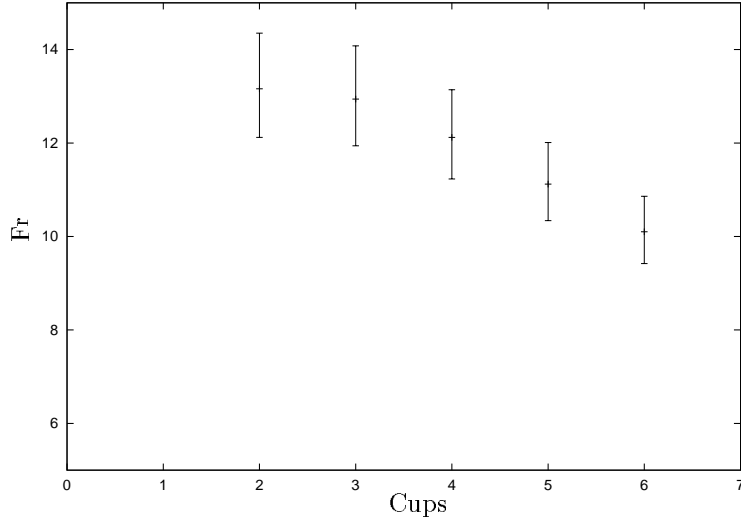
Figure 26: Change in the internal Froude number of the ballotini particle current for different mass of material released, measured at the end of the upper chute. One cup equals 0.4 kg of ballotini.

Experiment	runout, x [m]	x/x_{cont}	cm runout, $x^{cm}[m]$	x^{cm}/x^{cm}_{cont}
Low dam	1.09	0.89	0.58	0.73
Dam	0.92	0.75	0.43	0.55
High dam	0.75	0.61	0.33	0.42
Higher dam	0.65	0.53	0.25	0.32
Datum mounds	0.91	0.75	0.46	0.58
Narrow mounds 90°	0.81	0.66	0.41	0.52
Narrow mounds 60°	0.89	0.73	0.49	0.62
Narrow mounds 30°	0.96	0.79	0.55	0.69
Low mounds	0.99	0.81	0.55	0.69
High mounds	0.81	0.66	0.40	0.50
Smaller rel. area	1.0	0.82	0.63	0.79
Two rows	0.76	0.62	0.38	0.47
Trapizoidal	0.88	0.72	0.48	0.61
Conical mounds	0.98	0.80	0.59	0.75

Table 7: Summary of the experiments conducted. The runout was measured from where the row of obstacles was placed, x_{cont} is the runout of the control run, x^{cm} is the center of mass runout and $x^{cm}_{cont} = 0.79$ m, also measured from where the row of obstacles was placed.

might be slightly inaccurate (too high) since $u_0 = 2.6$ ms^{-1} was used. The semi-steady speed on the upper section of the chute was 2.7 ms^{-1} and is somewhat lower when the current hits
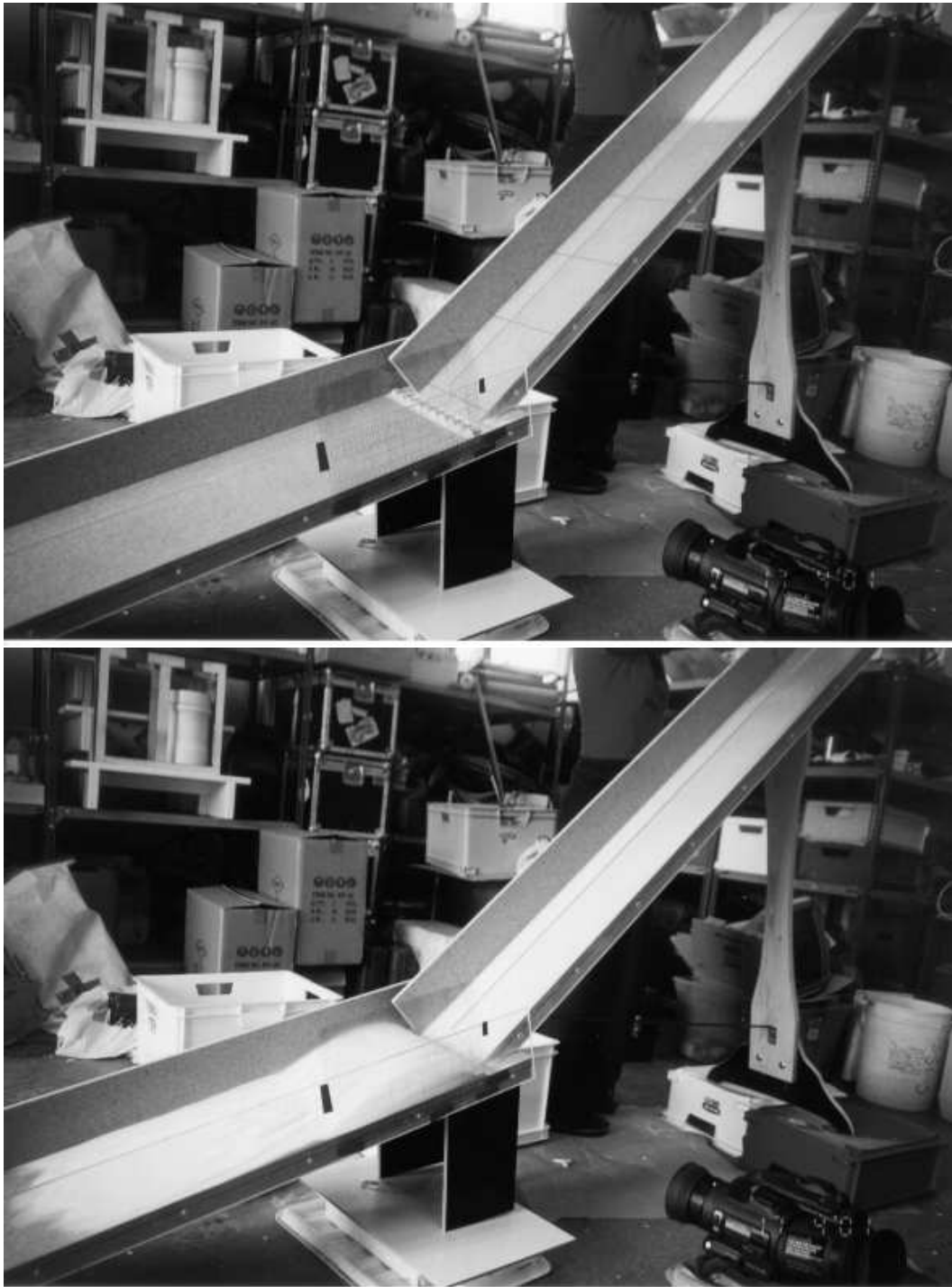
Figure 27: Photographs of the 3 m chute before and after the flow hits a row of trapizoidal mounds.
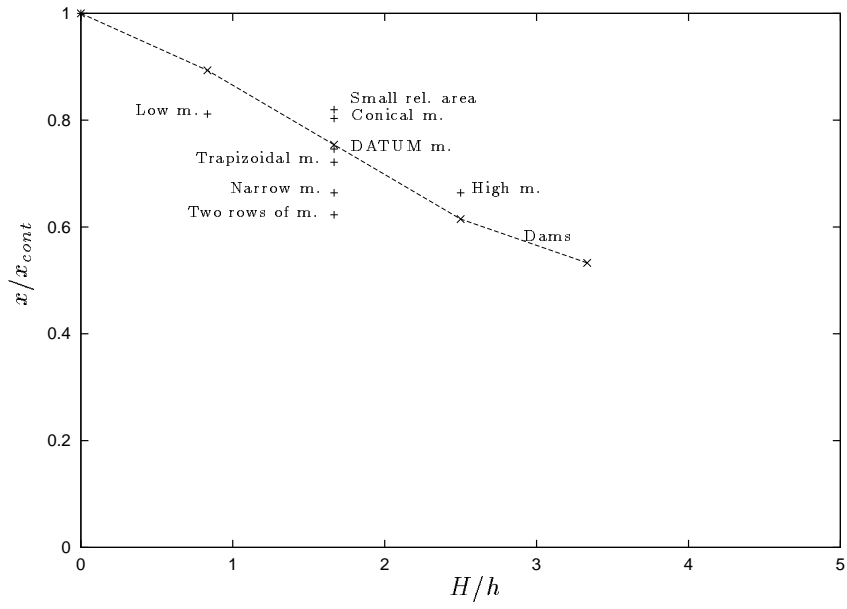
Figure 28: Non-dimensional runout, x/x_{cont} for the ballotini plotted against non-dimensional height of the obstacles, H/h.
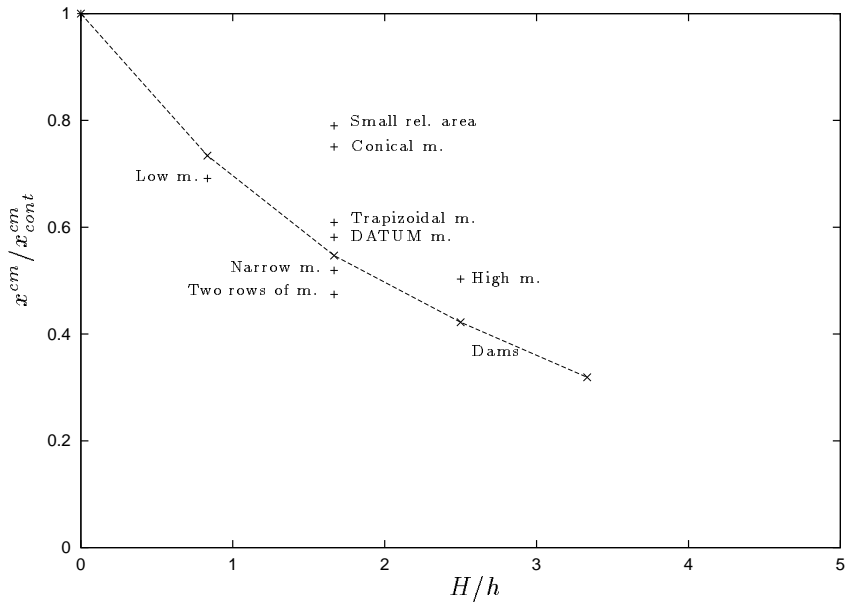
Figure 29: Non-dimensional centre of mass runout, x^{cm}/x_{cont}^{cm} for the ballotini plotted against non-dimensional height of the obstacles, H/h.
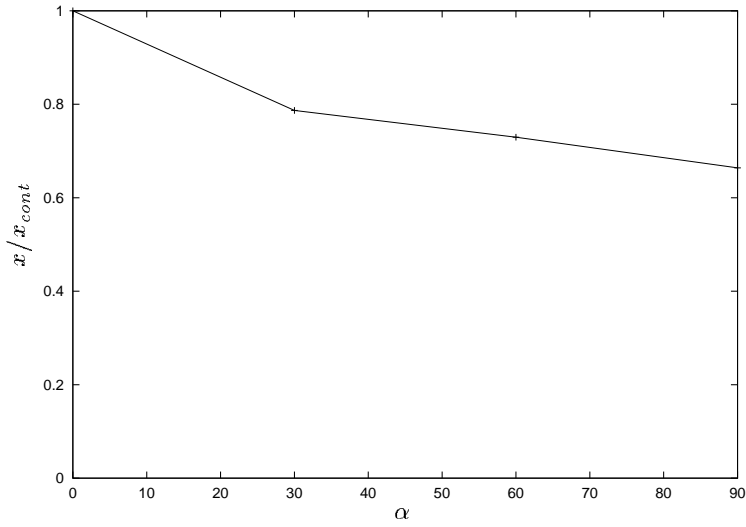
Figure 30: Non-dimensional runout, x/x_{cont} plotted against the angle between the upstream face of the mounds and the chute, α.
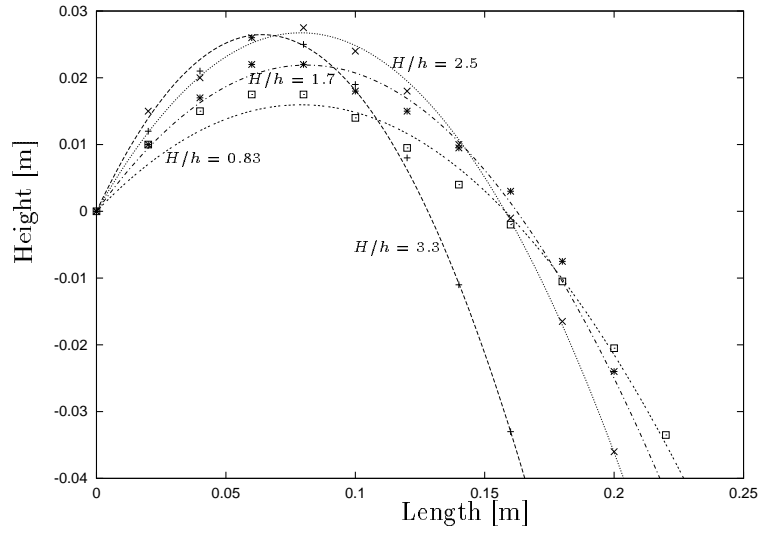
Figure 31: Jet profiles for 0.5, 1.0, 1.5 and 2.0 cm high dams.

the mounds since it has travelled on the less steep lower section of the chute for 2.5 cm. We were not able to measure the speed of the current just before hitting the mounds, so the speed used, 2.6 ms^{-1} is an estimate and might be too high. We see that an increase in the dam height leads to lowering of the velocity.
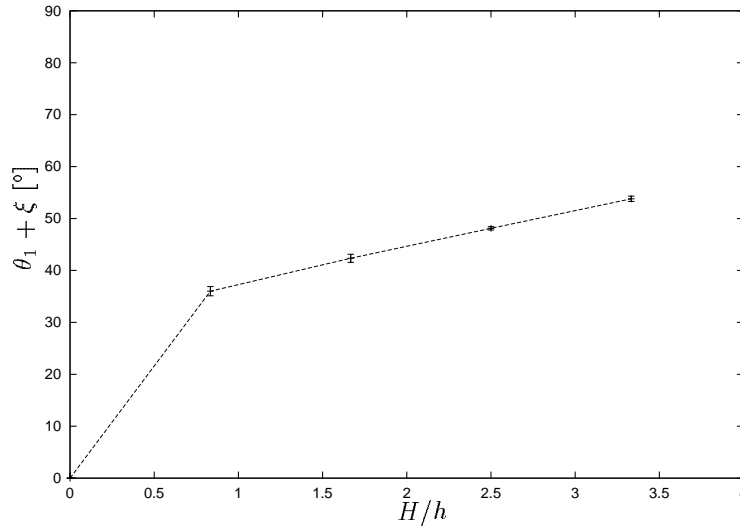
Figure 32: The throw angle, $\theta_1 + \xi$ plotted against the non-dimensional height of the obstacles, H/h, for the dams.
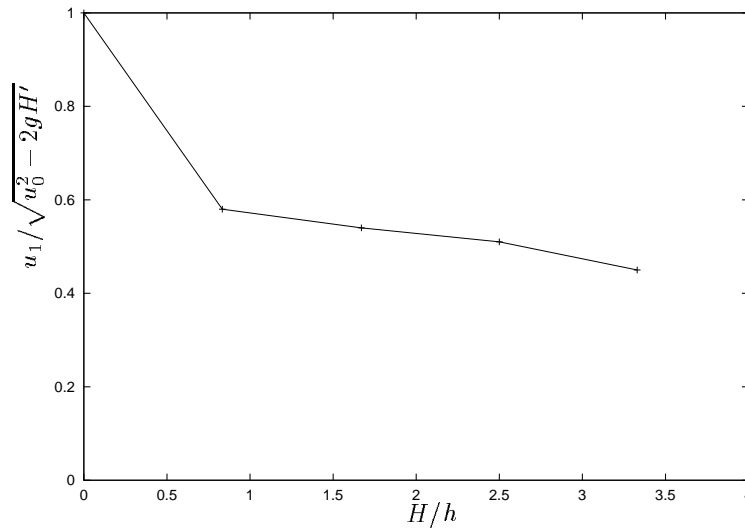
Figure 33: The ratio in equation (3) plotted against the non-dimensional height H/h for the dams.

4 Experiments at different scales compared

The experiments in Davos were in roughly twice the scale of the Bristol experiments, i.e. twice the flow height and thickness for the ballotini and sand experiments, but with the same internal Froude number of the order 10. The experiments performed in Reykjavík were in

about half the scale of the Bristol experiments. A summary of the material properties in these experiments is provided in Table 8.

Experiment	Material	ϕ [°]	δ [°]	d [mm]
Bristol	ballotini	$25 - 26$	$28 - 30$	0.1
Davos	ballotini	$21 - 23$	$17 - 18$	0.1
Davos	sand	$31.5 - 33.5$	$25 - 27.5$	2
Reykjavík	ballotini	$21 - 23$	$19 - 21$	0.1

Table 8: Material properties summarised, for the materials used in the experiments in Bristol, Davos and Reykjavík. The angle of repose is represented by ϕ, δ the dynamic bed friction angle and d is the mean particle diameter.

The Froude numbers of the flows on the upper sections of the chutes, using ballotini, were independent of the amount of material released for the Bristol and Davos experiments while the Reykjavík experiments showed some change in the Froude number.
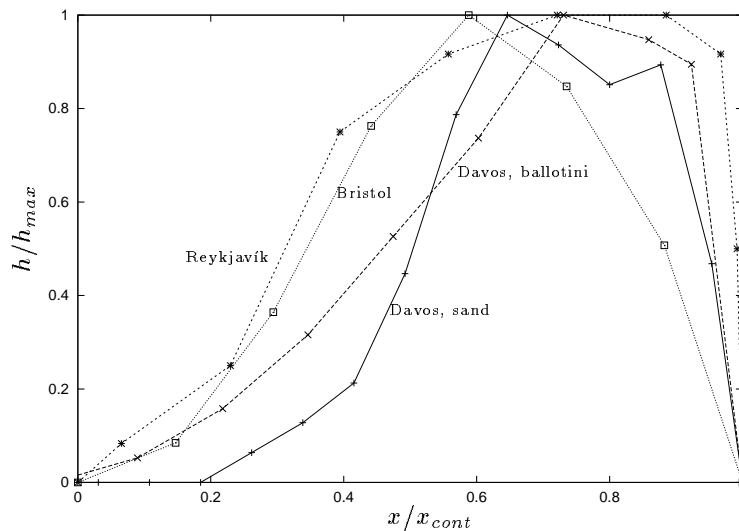
Figure 34: Averaged length profiles for the control runs without obstacles.

The averaged length profiles for the control runs without obstacles are plotted in Figure 34. The variations might be caused by the different frictional properties of the experimental materials and the chutes.

The datum mound configuration for the experiments in Bristol is shown in Figure 35. The shortening of the runout (Fig. 36) is broadly similar for the ballotini experiments at the three scales; for $H/h \leq 2$ the mounds are somewhat more effective than dams but when the mound height is increased further the dams become more effective. The most effective mound
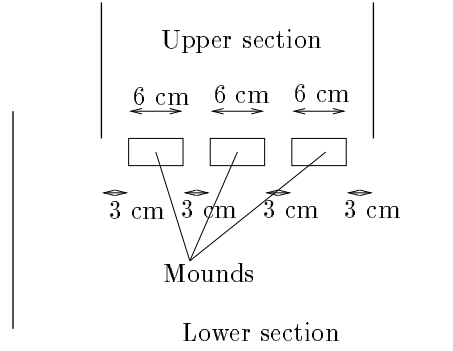
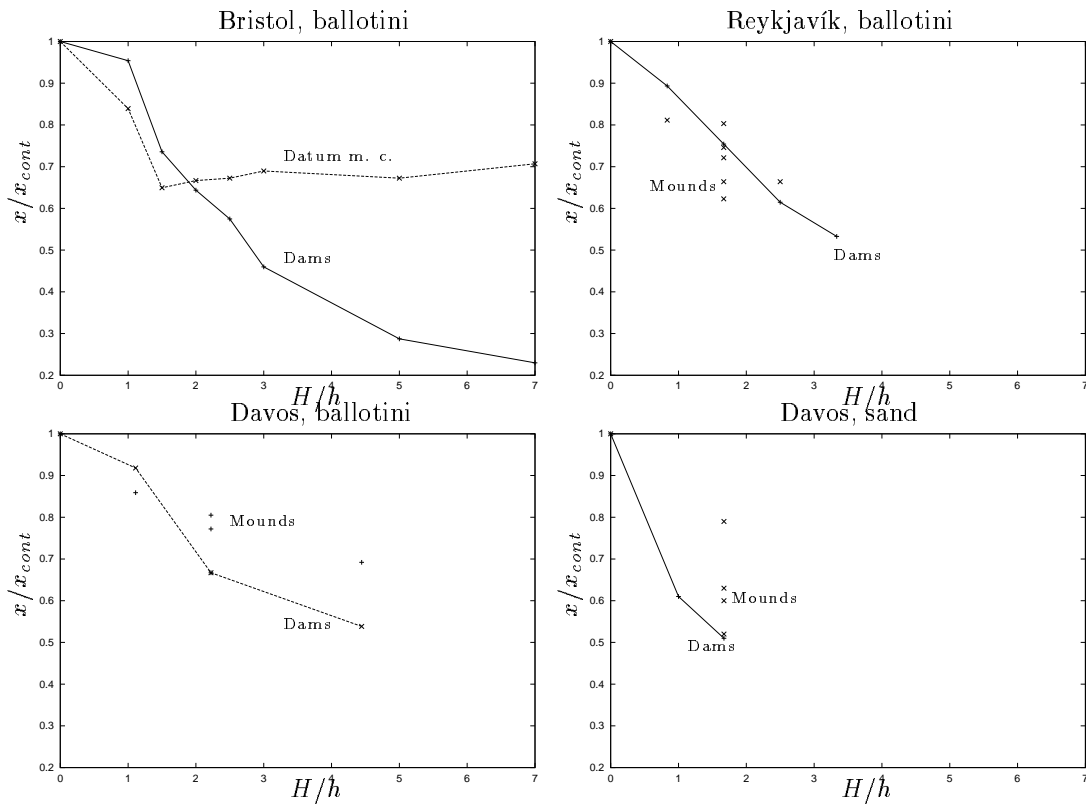Figure 35: Datum configuration of the mound geometry in Bristol, plan view.

Figure 36: Non-dimensional runout, x/x_{cont} plotted against non-dimensional heights of the obstacles, H/h. Datum m. c. stands for datum mound configuration and is defined in Fig. 35.

configuration shortens the maximum runout by about 30% for a single row of mounds. The sand experiments also show a similar trend. The most effective single row mound configuration shortens the maximum runout by about 40% and is approximately as effective as a dam of

the same height.
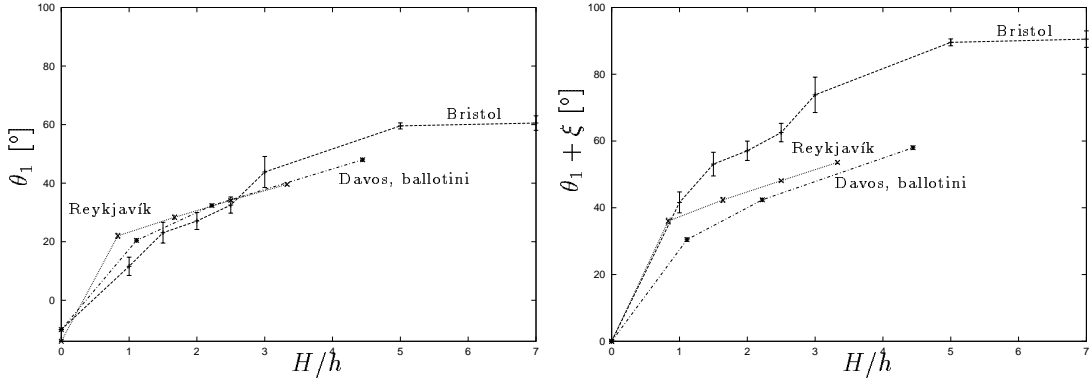
Figure 37: The throw angles θ_1 and $\theta_1 + \xi$ plotted against the non-dimensional heights of the dams.

The throw angle, θ_1, (the angle relative to the horizontal) was only analysed for the ballotini experiments and is plotted on the first graph in Figure 37 and the throw angle $\theta_1 + \xi$ (angle relative to the slope in which the mounds are situated) on the second graph.
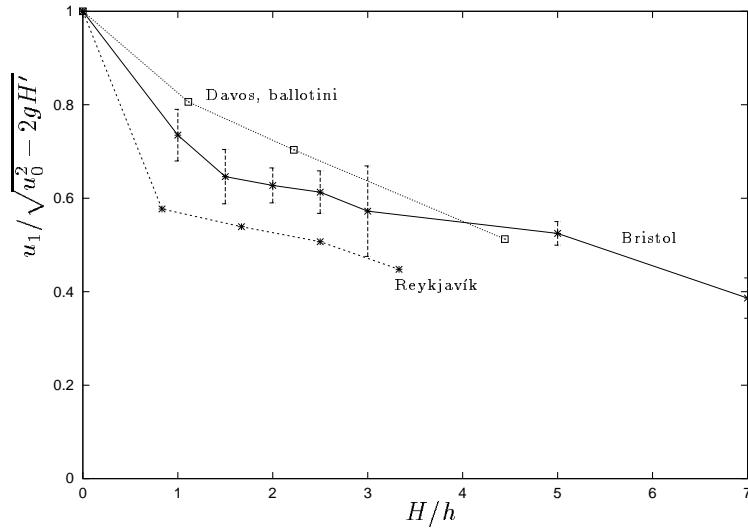
Figure 38: The ratio in equation (3) plotted against the non-dimensional heights of the dams.

Figure 38, displaying results for the ballotini experiments for dams, suggests that energy is dissipated in a broadly similar manner in the impact with the dams, for all laboratory scales. Thus, it appears that the speed reduction is a function of the non-dimensional height of the obstacles and not rapidly varying with the absolute scale of the flow over the obstacles. It seems reasonable to conclude that this result holds for substantially larger scales

than the scales of the laboratory experiments. More experiments at larger scales are though needed before one can conclude that these results also hold for the 10^2 larger scale of natural avalanches.

5 Conclusions

The main result of the experiments is that the shortening in the runout is very similar for all laboratory scales. Sand with completely different material properties and grain size also yields similar results. It may therefore be expected that the reported results hold to some approximation for substantially larger scales and different granular materials.

The experiments verify that breaking mounds have a considerable retarding effect on high Froude number granular currents. A substantial fraction of the kinetic energy of the oncoming flow is dissipated in the interaction of the flow with the mounds, including the launching of the jet and the subsequent landing of the jet and mixing with material flowing along the chute. Furthermore, a row of appropriately designed mounds has almost the same retarding effect as a continuous dam of the same height for non-dimensional obstacle heights up to 2. The energy dissipation depends on several aspects in the layout of the mounds. Specifically, we have examined the influence of the height of the mounds relative to the thickness of the oncoming stream, H/h, the steepness of the upper face of the mounds (only examined in Bristol), the height of the mounds relative to their width, H/B, the proportion of the cross sectional area of the impact zone covered by the mounds, A.

The following conclusions regarding the layout of the mounds can be drawn from the experiments in Davos and in Bristol:

1. $H/h \approx 2$: The proportion of the height of the mounds to the flow thickness. Increasing the height of the mounds any further does not lead to an additional reduction in the runout of the current. Note that snow accumulation on the ground, in the case of real snow avalanche protection measures, will lead to the need for somewhat higher mounds, typically $H/h \geq 3$.

2. The mounds should have steep upper faces.

3. $H/B \approx 1$: The proportion of the height of the mounds to their width (above the natural snowcover). For the same relative cross sectional area and height of the mounds, it is more effective to use mounds with a height to width ratio of approximately 1 than fewer and wider mounds.

4. A: The proportion of the flow path covered by mounds. Should be as large as possible and the gaps in between the mounds as small as possible. This is done to obtain maximum mixing of streams in the jet. In some cases a row of mounds can be more effective than a continuous dam with the same height (for a small ratio of H/h and certain mound configurations).

38

Acknowledgements

References

[1] J. D. Dent, K. J. Burrell, D. S. Schmidt, M. Y. Louge, and E. E. Adams. Density, velocity and friction measurements in a dry-snow avalanche. *Annals of Glaciology*, 26:247–252, 1998.

[2] K. M. Hákonardóttir. Retarding Effects of breaking Mounds. Avalanches. (M.Sc. thesis, University of Bristol), September 2000.

[3] A. W. Woods and A. J. Hogg. Snow avalanches. Models of particle-laden currents and avalanche protection measures. Centre for Environmental and Geophysical Research, School of Mathematics, University of Bristol, UK, 1998.

[4] A. W. Woods and A. J. Hogg. Experiments on granular flows passing over obstacles on an inclined chute. Centre for Environmental and Geophysical Research, School of Mathematics, University of Bristol, UK, August 1999.

A   Averaged length profiles - Davos

The averaged length profiles are plotted for each experiment and compared to the control run and the datum mound configuration.

A.1   Ballotini
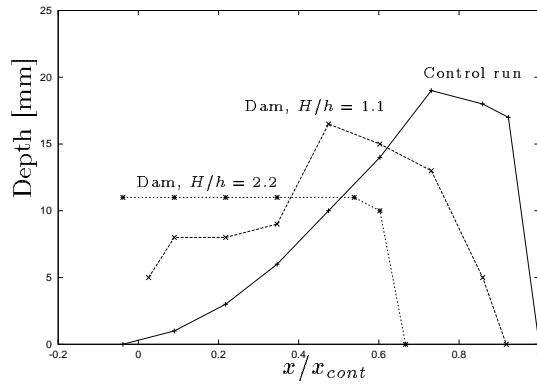
Figure 39: Averaged length profile for the dams.
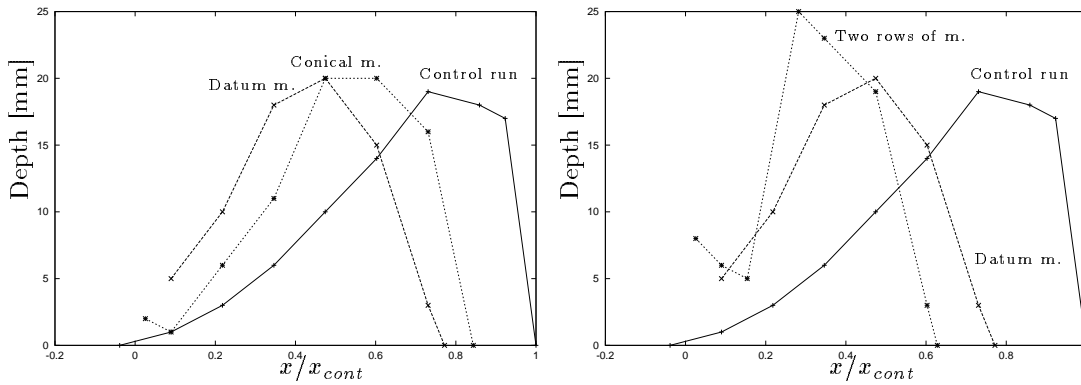
Figure 40: Averaged length profile for conical mounds and two rows of mounds.
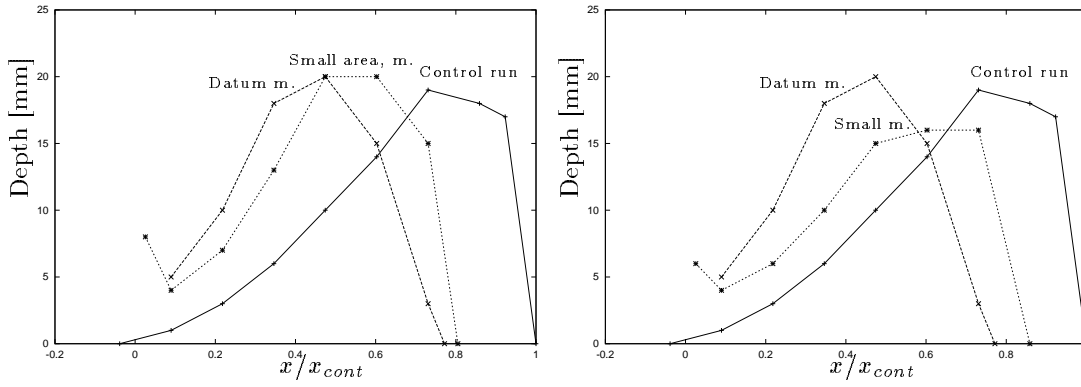
Figure 41: Averaged length profile for a smaller fraction of the area covered and smaller mounds.
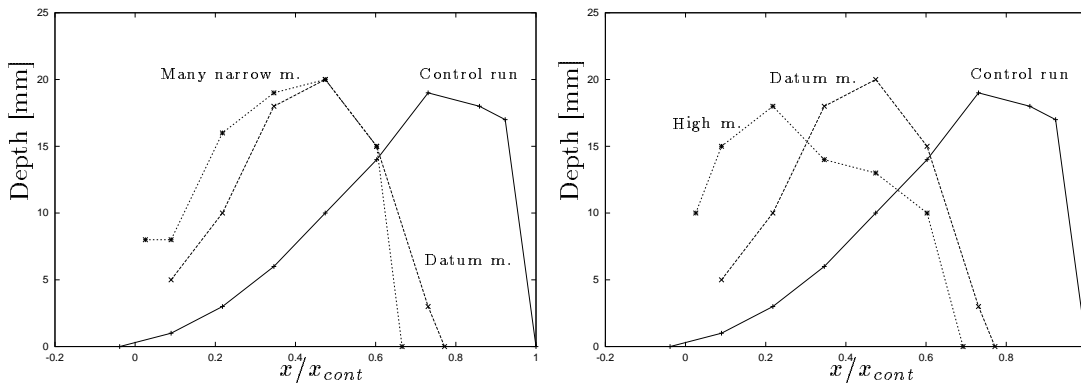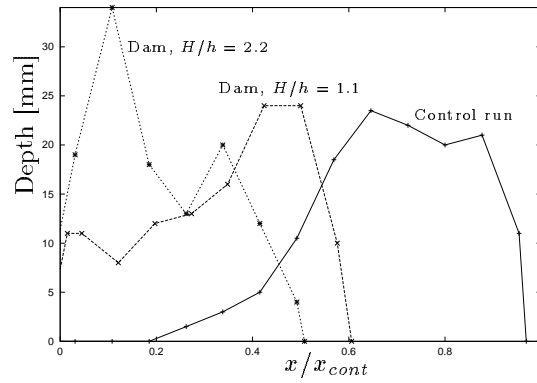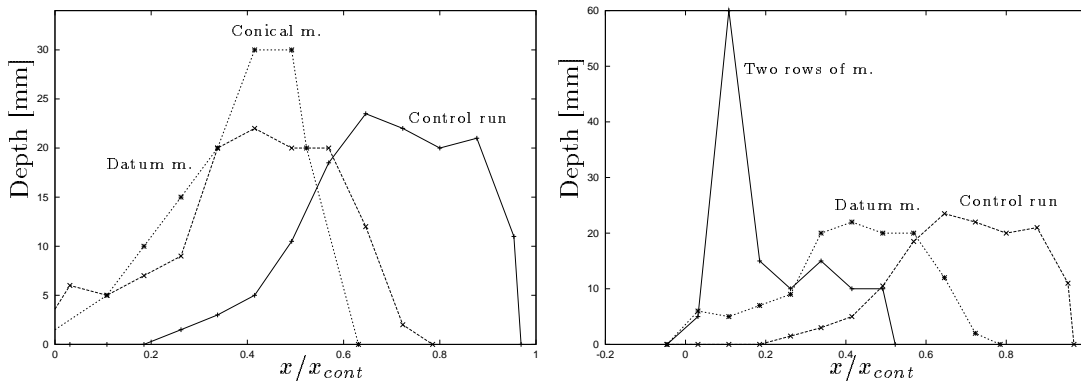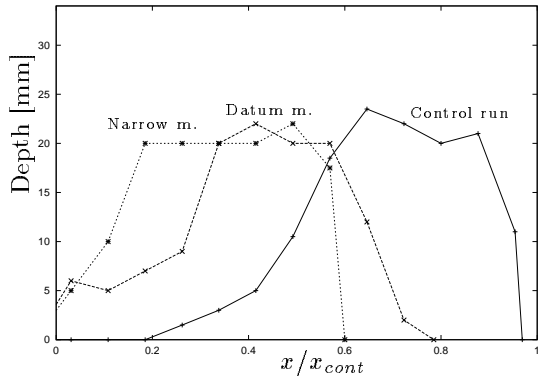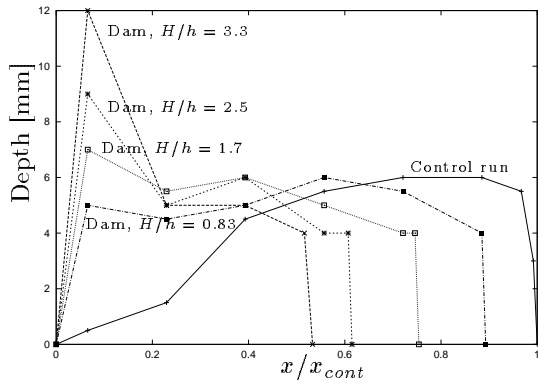

Figure 42: Averaged length profile for narrow mounds and high mounds.

A.2 Sand

Figure 43: Averaged length profile for the dams.

Figure 44: Averaged length profile for conical mounds and two rows of mounds.

42

Figure 45: Averaged length profile for narrow mounds.

B Averaged length profiles - Reykjavík

The averaged length profiles are plotted for each experiment and compared to the control run and the datum mound configuration. Ballotini was used in all the runs.
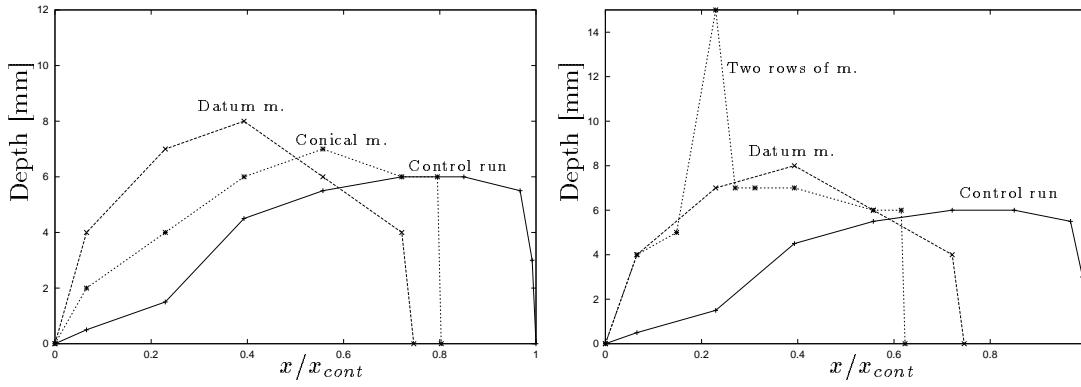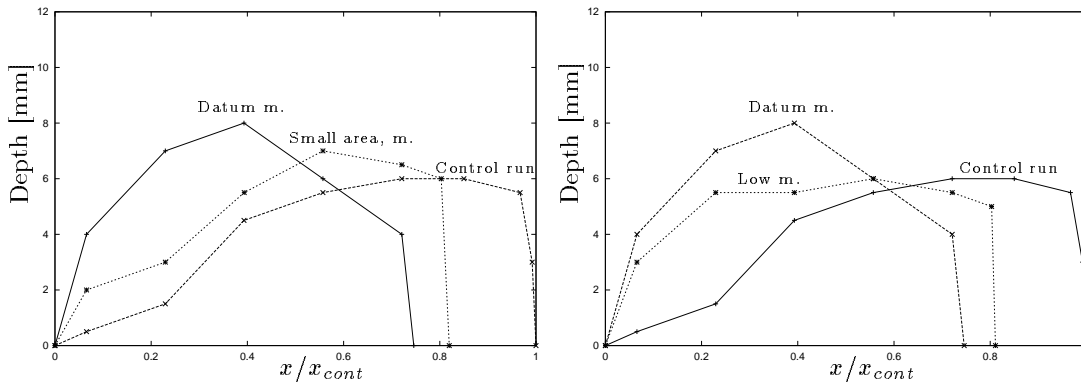

Figure 46: Averaged length profile for the dams.

43

Figure 47: Averaged length profile for conical mounds and two rows of mounds.

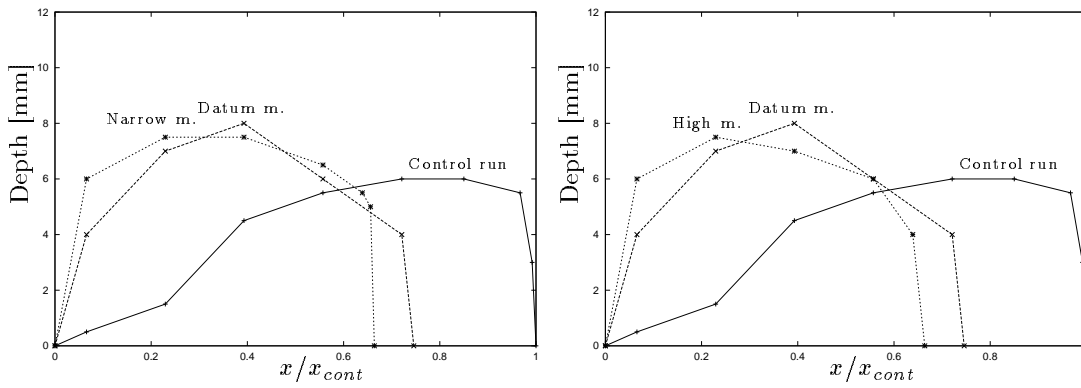Figure 48: Averaged length profile for a smaller fraction of the area covered and smaller mounds.

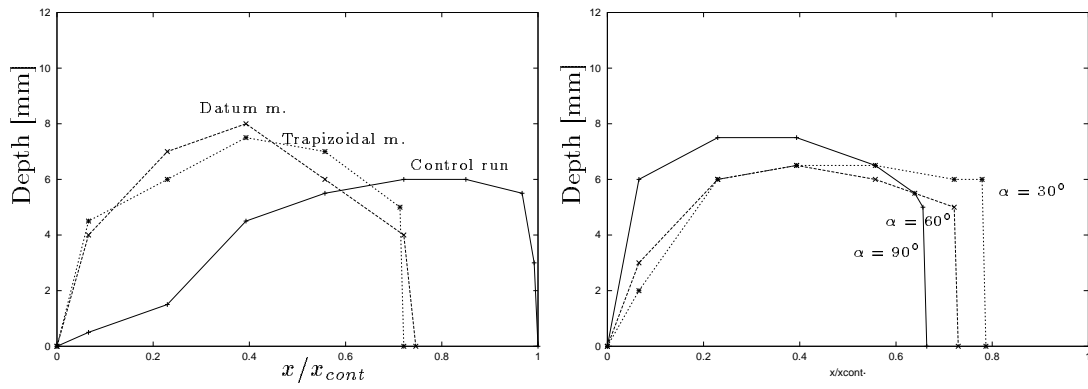Figure 49: Averaged length profile for narrow mounds and high mounds.

Figure 50: Averaged length profile for trapizoidal mounds and the narrow mounds with different upstream angles, α.